Discussion of Experimental Data for 3D Crack Propagation on the Basis of Three Dimensional Singularities

E. Schnack[1], W. Weber[2] and Y. Zhu[3]

Abstract: Three dimensional fracture mechanics was done by several groups in the past. One topic for these three dimensional fracture mechanics is to consider re-entrant corners or wedges for isotropic material. An algorithm was developed in the past to compute the dominant eigenvalues for those problems with high accuracy. Based on Kondratiev's Lemma for elliptic boundary value problems it is started with the asymptotic for the displacement and stress distribution around these three dimensional corners. By considering the mixed boundary value problem, the field quantities in the vicinity of corner points are computed by using a special finite element formulation, which is here the Petrov-Galerkin method. On that basis the quadratic eigenvalue problem is formulated and the dominant singularity exponent λ is determined iteratively by the Arnoldi method. Besides that, there are some new formulations in 3D crack propagation considering curved crack surfaces. They have been outlined as mode I, mode II and mode III formulations. In the fracture mechanics group of the University of Erlangen-Nuremberg, some experiments have been done especially for this 3D fracture mechanics effect at re-entrant corners. Therewith, the numerical data are compared with the experimental one. Moreover, the results are interpreted and it is shown that there are coincidences between theoretical and experimental results for re-entrant corners.

Keywords: Fracture mechanics, edge singularities, corner singularities, crack propagation

---

[1] Karlsruhe Institute of Technology (KIT), Institute of Solid Mechanics, Bldg. 10.91, 3rd Floor, Kaiserstr. 12, 76131 Karlsruhe, Germany. eckart.schnack@kit.edu

[2] Institute of Applied Mechanics, University Erlangen-Nuremberg,Egerlandstr. 5, 91058 Erlangen, Germany. weber@ltm.uni-erlangen.de

[3] Karlsruhe Institute of Technology (KIT), Institute of Solid Mechanics, Bldg. 10.91, 3rd Floor, Kaiserstr. 12, 76131 Karlsruhe, Germany. yao.zhu@kit.edu

1 Introduction

The start for this class of problems in 3D fracture is from a very famous paper by Benthem Benthem (1977). On the basis of Benthem's results, a lot of work has been done in this direction by Smith and his coworkers Smith et al (1986a,b); Smith and Kobayashi (1987) in the Virginia Polytechnic Institute of Technology. Besides the theoretical results by Benthem, the group of C. W. Smith has carried out a lot of experiments in 3D fracture. Very important is the remark of these papers: "The analytical origins of brittle fracture known as linear-elastic fracture mechanics analyses two-dimensional planar straight front cracks and did not account for situations where the stress-intensity factor varied along the crack front or when the crack front was curved or non-planar." From Benthem's results the equation is obtained.

$$U_{x_2} = Dr^{\lambda_u} \tag{1}$$

Here

U_{x_2} is the local displacement component normal to the local crack orientation.

r is the polar coordinate which originates from crack tip in the specimen slice(cf. Fig. 3).

λ_u is the lowest order eigenvalue.

D is a constant inside a plane normal to the crack surface and border($0 \leq \theta \leq \frac{\pi}{2}$), see Fig. 1.
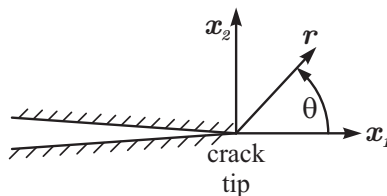
Figure 1: Crack tip and coordinate system

An experimental validation of the value of the dominant eigenvalue by Benthem has been done in Smith et al (1989) by the Moiré interferometry and by the frozen stress photoelasticity which is shown in Fig. 2.
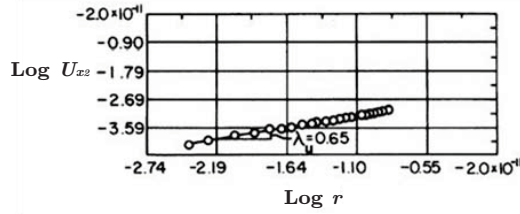
Figure 2: The slop for determining the dominant eigenvalue λ_u.

Additionally it is no problem to do this determination by using 3D finite element simulation, e.g. Schnack et al (1990). For this kind of problem the dominant eigenvalue λ_u for the surface is computed also as 0.65.

In Smith and Kobayashi (1986) the dominant eigenvalue in stress formulation is evaluated depending on the deepness of the specimen by photoelastic Moiré results together with the theoretical point from Benthem's result, cf. Fig. 3 and Fig. 4. Herein, the dominant eigenvalue in stress formulation λ_σ is defined by

$$\lambda_\sigma = |1 - \lambda_u| \tag{2}$$

after Benthem's equation has been scaled as:

$$\Rightarrow \log U_{x2} = \log D + \lambda_u \log r. \tag{3}$$
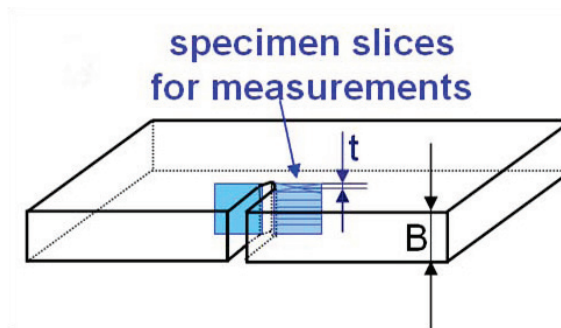
Figure 3: Specimen slices for measurements (t = distance of center of slice from the free surface).

Besides that the knowledge on corner singularities is very important especially for new materials like composites although there exists gap between experiments and theories.

As shown in Fig. 5 that the impact damage, the crack tips from the delamination, made cracks and crack tips from fiber/matrix debonding are observed.

For the classification of the singularity types, a very simple model problem with an internal crack and the intersection with a free surface of a homogenous isotropic elastic body is investigated as illustrated in Fig. 6.

For the edge singularity the stresses near the crack tip show the well-known asymptotic behavior from plain strain situation:

$$\sigma \sim \frac{1}{\sqrt{r}} \tag{4}$$

At the transition to the outer boundary a superposition of each edge and corner singularities is present. The dominant eigenvalue at that tip is at first unknown. Now, a full 3D problem has to be taken into account and at first this dominant eigenvalue λ has to be verified:

$$\sigma \sim \frac{1}{r^\lambda} \tag{5}$$

In the present paper it is started with the definition of the problem and then the asymptotics of the solution are discussed. From that the weak formulation of the problem is given and the finite element approximation of the problem is clarified.
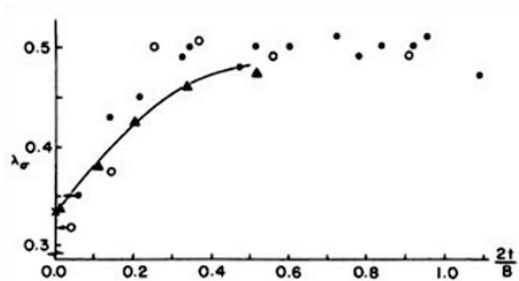
Figure 4: The dominant eigenvalue for these stress asymptotic depending on the parameter t normalized by the thickness of the specimen B.
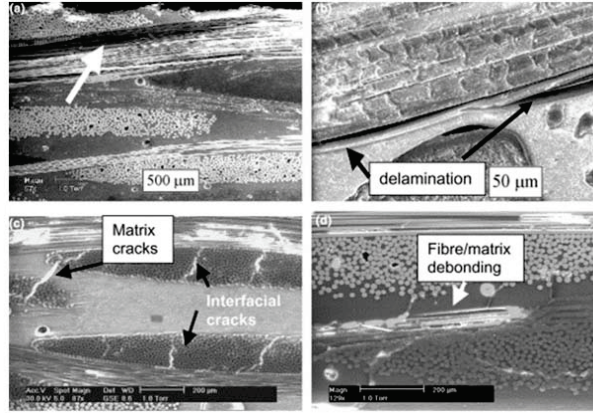
Figure 5: Impact damage in aramid-glass/epoxy composites: (a,b) near impact site; (c,d) in lower part of the sample Schnack (1990).

Then, the numerical solution of a quadratic eigenvalue problem is shown in the following. From that, 3D crack growth simulations are performed and finally the prediction of the kink angle is formulated.

2   Numerical treatment of singularities

At first, the set of equations for the 3D linear elasticity as a general mixed boundary value problem is defined as follows, with the matrix of elastic moduli $\mathbf{C}$ and the symmetric gradient operator in matrix form $\mathfrak{D}$ applied to the displacement vector $\mathbf{u}$ and the LAMÉ operator $\mathfrak{L}$. $\mathfrak{T}$ denotes the traction operator. The right hand side is given with f and the domain is $\Omega \subset \mathbb{R}^3$. Besides that, given displacement $\bar{\mathbf{u}}$ on $\partial\Omega_0$ and given tractions $\bar{t}$ on $\partial\Omega_1$ are prescribed:

$$\mathfrak{L}u := \mathfrak{D}^T \mathbf{C} \mathfrak{D}\mathbf{u} \;\; = \;\; f \quad \text{on} \quad \Omega \in \mathbb{R}^3 \tag{6a}$$

$$\mathbf{u} \;\; = \;\; \bar{\mathbf{u}} \quad \text{on} \quad \partial\Omega_0 \tag{6b}$$

$$\mathfrak{T}u := t(u) \;\; = \;\; \bar{t} \quad \text{on} \quad \partial\Omega_1 \tag{6c}$$

$\partial\Omega_0$ is the Dirichlet part of the boundary.

$\partial\Omega_1$ is the Neumann part of the boundary.

From the whole domain only the solution in the vicinity of the origin $\mathbf{O}$ is of special interest, see Fig. 7.
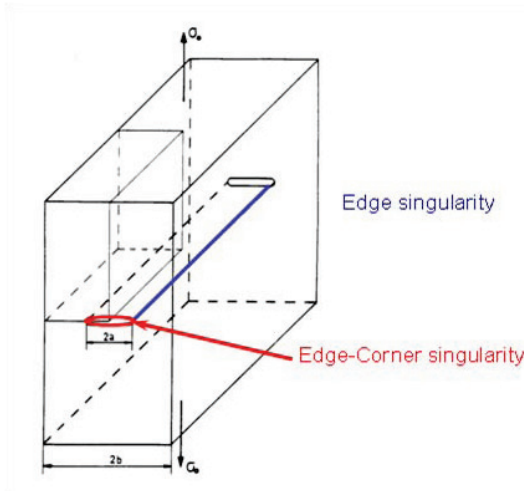
Figure 6: 3D simple model for edge corner singularity.

The cone $\mathscr{K}$ with the origin in O is given by the following equation:

$$\mathscr{K} := \left\{ x \in \mathbb{R}^3 : 0 < |x| < \infty, \quad \frac{x}{|x|} \in S \right\}.$$

By defining a sphere $\mathbb{S}^2$ as follows:

$$\mathbb{S}^2 \; in \; S \subset x \in \mathbb{R}^3 : |x| = 1,$$

the intersection S is obtained, cf. Fig. 7.

The boundaries of $\mathscr{K}$ and S consist of a Dirichlet part and a Neumann part. The Dirichlet part from the cone is $\partial \mathscr{K}_0$ and from S it is γ_0. Neumann part from the cone is at first $\partial \mathscr{K}_1$ and from S it is γ_1 with the side conditions.

Boundaries of $\mathscr{K}$ and S:

Dirichlet parts $\partial \mathscr{K}_0$ and γ_0

Neumann parts $\partial \mathscr{K}_1$ and γ_1

With

$$\partial \mathscr{K}_0 \cap \partial \mathscr{K}_1 \;\; = \;\; 0, \quad \gamma_0 \cap \gamma_1 = 0 \tag{7}$$

$$\partial \mathscr{K}_0 \cup \partial \mathscr{K}_1 \;\; = \;\; \partial K, \quad \gamma_0 \cup \gamma_1 = S \tag{8}$$
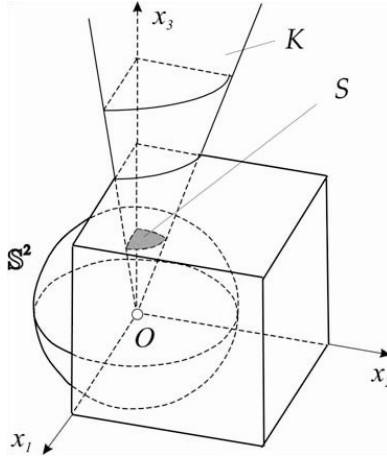
Figure 7: Crack tip definition with sphere $\mathbb{S}^2$ and cone K.

Next, an ε-ball around O is defined by

$$U_O^\varepsilon := \{x \in \mathbb{R}^3 : 0 < |x| < \varepsilon\}. \tag{9}$$

The intersection of the cone $\mathscr{K}$ with the ε-ball U_O^ε is given by (see Fig. 8)

$$\{\Omega_O^\varepsilon := \mathscr{K} \cap U_O^\varepsilon = \Omega \cap U_O^\varepsilon\}. \tag{10}$$

The boundaries of Ω_O^ε are the Dirichlet part Γ_0 and the Neumann part Γ_1. Additionally, a transmission boundary exists,

$$\Gamma_T = \partial \Omega_O^\varepsilon \backslash (\Gamma_0 \cup \Gamma_1) \tag{11}$$

where the given Dirichlet data $\bar{u}$ and the given traction data $\bar{t}$ are transduced via Γ_T in direction of the origin O.

Now, the local properties of solution of Eq. (6) only in the vicinity of O are of interest. Therefore, an equivalent mixed boundary value problem on Ω_O^ε is defined in the following.

It is assumed that only homogeneous boundary values on the subdomain Ω_O^ε are prescribed. Otherwise, additional singularities will occur in the 3D problem, which are neglected in the following studies. At the transmission boundary $|\mathbf{x}| = \varepsilon$ the Dirichlet conditions u are û, which are taken from solution of Eq. (6). Therefore, the following equation system for the mixed boundary value problem has to be
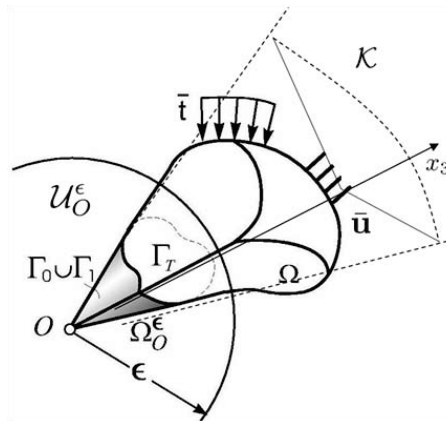
Figure 8: The $\varepsilon-$ball around O.

solved:

$$\mathfrak{L}u \;=\; f \quad on \quad \Omega_0^\varepsilon \tag{12a}$$

$$u \;=\; \hat{u} \quad on \quad \Gamma_T \tag{12b}$$

$$u \;=\; 0 \quad on \quad \Gamma_0 \tag{12c}$$

$$\mathfrak{T}u \;=\; 0 \quad on \quad \Gamma_1 \tag{12d}$$

According to the results in Kondratiev (1967) the solution $u(r,\theta,\varphi)$ of Eq. (12) in the vicinity of the origin O is written in following asymptotic expansion:

$$u(r,\theta,\varphi) = \sum_i \sum_{k=0}^{k_i} K_{ik} r^{\lambda_i} \ln^k r \, \mathbf{U}_{ik}(\theta,\varphi) \tag{13}$$

with

λ_i – the singular exponents,

k_i of λ_i – the algebraic multiplicity,

$\mathbf{U}_{ik}(\theta,\varphi)$ – the generalized eigenvectors,

K_{ik} – the generalized stress intensity factors.

Now, the singular exponents λ_i as well as the eigenvectors $\mathbf{U}_{ik}(\theta,\varphi)$ have to be computed. The physical interpretation of the so-called generalized stress intensity

factors K_{ik} is in general totally unknown. Therefore, these confusions have only a formal status for the following and these values are interpreted only for special cases in fracture mechanics.

The local property of the solution of Eq. (12) in Ω_0^ε is studied in a model problem for the whole cone $\mathcal{K}$ by applying the perturbation theory, and with this theory the mapping $\Upsilon = \varepsilon^{-1}x$ is utilized.

With this initial formulation, the ε-ball Ω_0^ε is zoomed on the whole cone $\mathcal{K}$ by taking the limit $\varepsilon \to 0$. Therefore, the right hand side f of Eq. (12) vanishes from the given equation set. Therewith, only the second derivatives remain in the LAMÉ operator and the model problem is written as

$$\mathfrak{L}u \;=\; 0 \quad on \quad \mathcal{K} \tag{14a}$$

$$u \;=\; 0 \quad on \quad \partial\mathcal{K}_0 \tag{14b}$$

$$\mathfrak{T}u \;=\; 0 \quad on \quad \partial\mathcal{K}_1 \tag{14c}$$

So for that, the Dirichlet part is defined by

$$\partial\mathcal{K}_0 = \{x \in \partial\mathcal{K} : x/|x| \in \gamma_0\} \tag{15}$$

and the Neumann part of the boundary by

$$\partial\mathcal{K}_1 = \{x \in \partial\mathcal{K} : x/|x| \in \gamma_1\} \tag{16}$$

Now the problem is reduced from 3D to a 2D one which exists only on the surface of the sphere and is written as

$$\mathbf{u}(r,\theta,\varphi) = r^\lambda \mathbf{U}(\theta,\varphi) \tag{17}$$

in spherical coordinates.

The reason for the reduction is that the first term in the Taylor expansion of Kondratiev's result is a log term, see Eq. (13). Since only a small region round the origin O is under consideration the log term i.e. $\ln^k r$ is nearly constant for small r. Therefore this term can be neglected and only the term r^λ has to be considered. The spectral problem corresponding to Eq. (14) is the following:

$$\mathbf{U} = U(\theta,\varphi)\mathbf{e}_x + V(\theta,\varphi)\mathbf{e}_y + W(\theta,\varphi)\mathbf{e}_z \tag{18}$$

For this equation set has to be solved in the following:

$$\mathfrak{L}\left(\partial_\theta,\partial_\varphi;\lambda\right)U \;=\; 0 \quad on \quad S \tag{19a}$$

$$U \;=\; 0 \quad on \quad \gamma_0 \tag{19b}$$

$$\hat{\mathfrak{T}}\left(\partial_\theta,\partial_\varphi;\lambda\right)U \;=\; 0 \quad on \quad \gamma_1 \tag{19c}$$

In summarizing, this is spectral problem where λ denote the eigenvalues.

To find the solution of this problem, a weak formulation for this spectral problem is requested. So, looking for functions in the Sobolev space for the test function:

$$\left[\mathbb{H}_0^1 \left(\Omega_0^\varepsilon \right) \right]^3 := \left\{ \mathbf{v} \in \left[\mathbb{H}^1 \left(\Omega_0^3 \right) \right]^3 : \mathbf{v} = 0 \; on \; \Gamma_0 \cup \Gamma_T \right\} \tag{20}$$

The weak formulation of the problem is now to find $\mathbf{u} \in \left[\mathbb{H}^1 \left(\Omega_0^3 \right) \right]^3$ so that the bilinear form holds:

$$\mathscr{B} \left(\mathbf{u}, \mathbf{v} \right) := 0, \quad \forall \quad \mathbf{v} \in \left[\mathbb{H}^1 \left(\Omega_0^3 \right) \right]^3 \tag{21}$$

The bilinear form is produced by stresses and strains:

$$\mathscr{B} \left(\mathbf{u}, \mathbf{v} \right) := \int_{\Omega_0^\varepsilon} \sigma^T \left(\mathbf{u} \right) \varepsilon \left(\mathbf{v} \right) \mathrm{d}\Omega \tag{22}$$

In this bilinear form the Cauchy stress tensor is defined by

$$\sigma^T = \left[\sigma_x, \sigma_y, \sigma_z, \tau_{yz}, \tau_{xz}, \tau_{xy} \right] \tag{23}$$

and the linearized strains tensor by

$$\varepsilon^T = \left[\varepsilon_x, \varepsilon_y, \varepsilon_z, 2\varepsilon_{yz}, 2\varepsilon_{xz}, 2\varepsilon_{xy} \right] \tag{24}$$

Looking for the weak formulation in the Sobolev space $\left[\mathbb{H}^1 \left(\Omega_0^\varepsilon \right) \right]^3$ by assuming a solution

$$\mathbf{u} \left(r, \theta, \varphi \right) = r^\lambda \mathbf{U} \left(\theta, \varphi \right) \tag{25}$$

a finite elastic strain energy has to be ensured. This means

$$\int_{\Omega_0^\varepsilon} |\mathbf{u}|^2 \mathrm{d}\Omega < \infty \tag{26}$$

and

$$\int_{\Omega_0^\varepsilon} |\nabla \mathbf{u}|^2 \mathrm{d}\Omega < \infty \tag{27}$$

From that the final integral is obtained:

$$\int_0^\varepsilon r^{2\lambda-2} r^2 \mathrm{d}r = \left[\frac{r^{2\lambda+1}}{2\lambda+1} \right]_0^\varepsilon < \infty \Rightarrow \lambda > -\frac{1}{2} \tag{28}$$

Here only the singular part of the solution is of interest. Therefore the real part of the eigenvalue λ has to be part of the following open interval: $-\frac{1}{2} < \mathrm{Re}\,(\lambda) < 1$. It is assumed that these bounds for the real part of λ are also correct, if the log term $\ln^k r$ in Kondratiev's result is also considered.

3 Resulting eigenvalue problem

Because different trial and test functions are applied, the Petrov-Galerkin finite element method is utilized.

The trial functions are given by

$$U_h := \mathrm{span}\left\{ r^\lambda \mathbf{w}_i\,(\theta,\varphi)\,;\, i = 1,...,M \right\} \subset \left[\mathbb{H}^1\,(\Omega_0^\varepsilon) \right]^3 \tag{29}$$

and the test functions by

$$V_h := \mathrm{span}\left\{ \Phi\,(r)\,\mathbf{w}_i\,(\theta,\varphi)\,;\, i = 1,...,M \right\} \subset \left[\mathbb{H}_0^1\,(\Omega_0^\varepsilon) \right]^3 \tag{30}$$

with $\{\mathbf{w}_i\,(\theta,\varphi)\,;\, i = 1,...,M\}$ as the usual basis of finite dimensional subspaces of $\left[\mathbb{H}^1\,(S) \right]^3$ with

$$\mathbf{w_i}(\theta,\varphi) = \begin{cases} 1 & \text{in node}(\theta_i, \varphi_i) \tag{31} \\ 0 & \text{else.} \tag{32} \end{cases}$$

Now, the solution as a finite element approximation in a weak form $\mathbf{u}^h \in U_h \subset \left[\mathbb{H}^1\,(\Omega_0^\varepsilon) \right]^3$ is produced such that

$$\mathcal{B}\,(\mathbf{u},\mathbf{v}) := 0, \quad \forall \mathbf{v}^h \in V_h \subset \left[\mathbb{H}^1\,(\Omega_0^3) \right]^3 \tag{33}$$

The finite element system with a vector of displacements gives us the following quadratic eigenvalue problem:

$$\left[(\mathbf{K} - \mathbf{D}) + \lambda\,(\mathbf{D^T} - \mathbf{D} - \mathbf{M}) + \lambda^2 \mathbf{M} \right]^T \mathbf{d} = \mathbf{0} \tag{34}$$

with the definition of the stiffness matrix:

$$\mathbf{K} = \sum_{i=1}^{N} \mathbf{T}_d^{-T} \int_i \mathbf{F}_0^T \mathbf{T}_\varepsilon^T \mathbf{CT}_\varepsilon \mathbf{F}_0 \sin\theta \, d\theta \, d\varphi \, \mathbf{T}_d^{-1} \tag{35}$$

and the damping matrix:

$$\mathbf{D} = \sum_{i=1}^{N} \mathbf{T}_d^{-T} \int_i \mathbf{F}_0^T \mathbf{T}_\varepsilon^T \mathbf{CT}_\varepsilon \mathbf{F}_1 \sin\theta \, d\theta \, d\varphi \, \mathbf{T}_d^{-1} \tag{36}$$

and finally the mass matrix:

$$\mathbf{M} = \sum_{i=1}^{N} \mathbf{T}_d^{-T} \int_i \mathbf{F}_1^T \mathbf{T}_\varepsilon^T \mathbf{CT}_\varepsilon \mathbf{F}_1 \sin\theta \, d\theta \, d\varphi \, \mathbf{T}_d^{-1} \tag{37}$$

In this formulation $\mathbf{T}_d$, $\mathbf{T}_\varepsilon$ are Boolean matrices for rearranging displacements and strains. $\mathbf{F}_0$, $\mathbf{F}_1$ are matrices with gradients of the displacements and with parts of the Jacobian matrix. For the numerical solution of the quadratic eigenvalue problem for the unknowns λ three steps are performed:

1. In the first step the mapping: $\bar{\lambda} = \lambda - \frac{1}{2}$ is used which yields

$$\left[\mathbf{P} + \bar{\lambda}\mathbf{Q} + \bar{\lambda}^2\mathbf{R}\right]\mathbf{d} = \mathbf{0} \tag{38}$$

Here $\mathbf{P}, \mathbf{R}$ are symmetric operators and $\mathbf{Q}$ is a skew symmetric operator.

2. A linearization of the problem by introducing the new vector $\mathbf{x}$ is performed such that $\bar{\lambda}\mathbf{x} = \bar{\lambda}^2\mathbf{Rd}$ is obtained. Therewith, the linear eigenvalue problem for $\bar{\lambda}$ reads as:

$$\begin{bmatrix} \mathbf{P} & \mathbf{0} \\ \mathbf{0} & \mathbf{I} \end{bmatrix} \begin{bmatrix} \mathbf{d} \\ \mathbf{x} \end{bmatrix} = \bar{\lambda} \begin{bmatrix} -\mathbf{Q} & -\mathbf{I} \\ \mathbf{R} & \mathbf{0} \end{bmatrix} \begin{bmatrix} \mathbf{d} \\ \mathbf{x} \end{bmatrix} \tag{39}$$

where I is the identity matrix.

3. The formulation till now is fast for the biggest eigenvalues of the problem. However, the denominator means the smallest eigenvalue of that problem is

of special interest. Therefore, another mapping $\theta = \bar{\lambda}^{-1}$ with the side condition $0 < \text{Re}\bar{\lambda} = 0.5 + \text{Re}\lambda < 1.5$ is utilized. Therewith, the final formulation

$$(\mathbf{X} - \theta\mathbf{I}) \begin{bmatrix} \mathbf{d} \\ \mathbf{x} \end{bmatrix} = \mathbf{0} \tag{40}$$

is obtained where

$$\mathbf{X} = \begin{bmatrix} \mathbf{P} & \mathbf{0} \\ \mathbf{0} & \mathbf{I} \end{bmatrix}^{-1} \begin{bmatrix} -\mathbf{Q} & -\mathbf{I} \\ \mathbf{R} & \mathbf{0} \end{bmatrix} \tag{41}$$

The final system Eq. (40) is solved by an iterative scheme based on the Arnoldi method. The reasons for that are very clear:

- Computational effort is only $\mathcal{O}(n)$ instead of $\mathcal{O}(n^2)$ for 2D Gaussian elimination on band matrices (n denotes the dimension of matrices $\mathbf{P}$, $\mathbf{Q}$ and $\mathbf{R}$)

- The memory used is proportional to $2n \cdot \mathcal{O}(k) + \mathcal{O}(k^2)$ instead of $\mathcal{O}(n^{3/2})$ for 2D Gaussian elimination on band matrices ($k << n$ denotes dimension of Krylov subspace).

- The eigenvectors of the problem can be obtained practically without additional effort.

The general idea of the Arnoldi method is to create Krylov subspace with given start vector $\mathbf{y}$: $K_k(\mathbf{X}, \mathbf{y}) := \text{span}\left\{\mathbf{y}, \mathbf{X}\mathbf{y}, ..., \mathbf{X}^{k-1}\mathbf{y}\right\}$ with $\dim(K_k(\mathbf{X}, \mathbf{y})) = k > 1$ and now find the best approximation of the eigenvectors of $\mathbf{X}$ within $K_k(\mathbf{X}, \mathbf{y})$.

The calculation of the Krylov subspaces is performed in two steps. At first, the vector $\mathbf{z}$ as a function on $\mathbf{y}$ is defined as $\mathbf{z} = \mathbf{X}\mathbf{y}$ for a given $\mathbf{y} = (\mathbf{y_1}, \mathbf{y_2})^T$. Without any explicit calculation of $\mathbf{X} \in \mathbb{R}^{2n \times 2n}$ the first computation step is

$$\begin{bmatrix} \mathbf{w_1} \\ \mathbf{w_2} \end{bmatrix} := \begin{bmatrix} -\mathbf{Q} & -\mathbf{I} \\ \mathbf{R} & \mathbf{0} \end{bmatrix} \begin{bmatrix} \mathbf{y_1} \\ \mathbf{y_2} \end{bmatrix} = \begin{bmatrix} -\mathbf{Q}\mathbf{y_1} - \mathbf{y_2} \\ \mathbf{R}\mathbf{y_1} \end{bmatrix}. \tag{42}$$

And the second step is

$$\mathbf{z} = \begin{bmatrix} \mathbf{P}^{-1}\mathbf{w_1} \\ \mathbf{w_2} \end{bmatrix}. \tag{43}$$

4 Numerical tests for fracture mechanics problems

Before physical problems in fracture are analyzed, the computation time for the eigenvalue problem especially for the problems with a high number of degrees of freedom is under consideration.

Table 1: Process data on an IBM-6000, with 77 power2 processors in 2 GB RAM

Typical values for calculation	
Degree of freedom:	231,840
Dimension of KRYLOV subspace	20
Time for solving(42)	6min 51.4s
Time for:$P \rightarrow LU$	5 min 54.5s
Memory usage:	770MB

From Table 1 it can be seen that the results of the problems with more than 200,000 unknowns are calculated in less than 7 minutes CPU.

As a Benchmark problem for the analysis of the convergence of the numerical solution, a semi-infinite plane crack as illustrated in Fig. 9 is utilized.
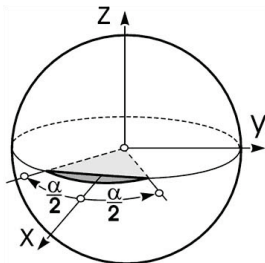
Figure 9: Benchmark problem: Spherical coordinates.

Since it is a symmetric problem and the dimension of the problem has been reduced from a 3D to a 2D one, only the dashed area has to be discretised (cf. Fig. 10, where *D* is the distance from the middle of crack to to the end of crack, *S* is the distance parameter from crack to free surface). In Fig. 11 the used coarse mesh for the calculation of the eigenvalues is plotted and Fig. 12 shows the fine mesh, which is black around the crack tip.

In Fig. 13 the convergence ratio *p* for different element types is shown. Besides a linear approximation in the shape functions with an equally refined mesh, better results are obtained by using also a linear approximation in the shape functions but
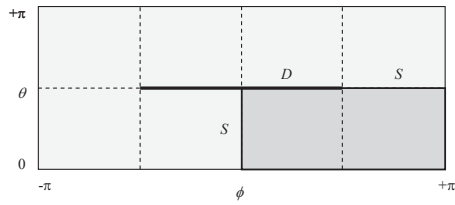
Figure 10: Domain to be discretised.
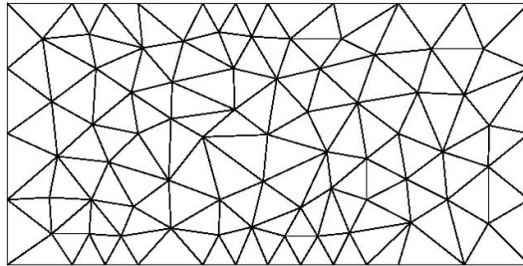
Figure 11: Coarse mesh used.
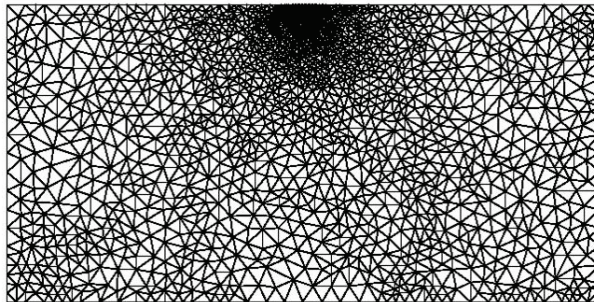
Figure 12: Finest mesh used, which is black around the crack tip.
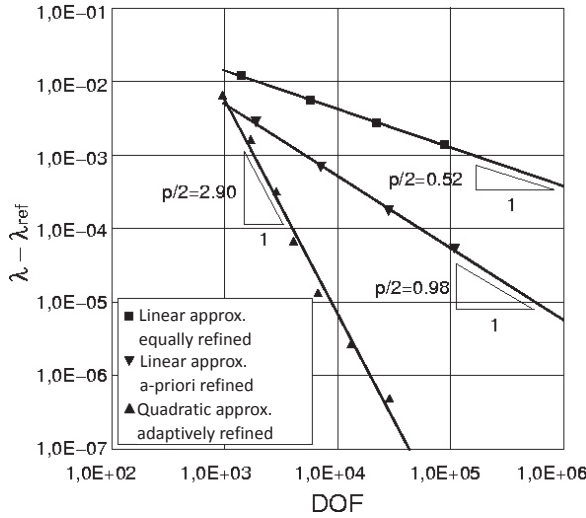
Figure 13: Convergence rates as $|\lambda - \lambda_{ref}| \sim h^p$, h is mesh parameter.

with an a-priori refinement. The best results – as expected – are calculated by using a quadratic approximation of the shape function with an adaptive refinement for the mesh. Compared to the reference dominant eigenvalue λ_{ref} Apel (2001) a very high accuracy in Fig. 13 is observed.

For the asymptotic analysis of the stress intensity factor $k(z)$ on the crack front, two asymptotical presentations of the displacements are used. The first one is outlined in cylindrical coordinates for points at a smooth part of the crack front and reads as

$$\mathbf{u}_P(\rho, \phi, z) = k(z)\rho^{1/2}\hat{\mathbf{u}}(\varphi) + O(\rho^{\eta}), \ \eta > \frac{1}{2} \tag{44}$$

where

k stress intensity factor (SIF)

$\hat{\mathbf{u}}$ angular function

Additionally, the formulation

$$\mathbf{u}_P(r, \theta, \varphi) = Kr^{\lambda}\hat{\mathbf{U}}(\theta, \varphi) + O(r^{\mu}), \ \mu > \lambda \tag{45}$$

in spherical coordinates for the singular point O is used, where

K corner stress intensity factor (CSIF),
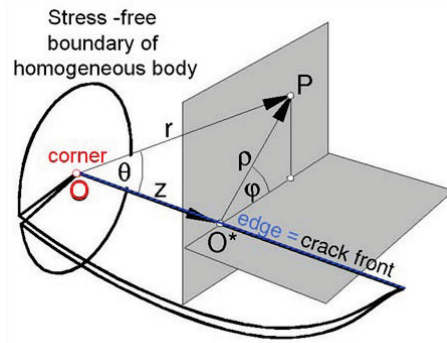
Figure 14: Displacement in a point P.

$\hat{U}$ angular function,

λ corner singularity (complex number in general).

By the utilization of the relationship of the coordinates $r = \frac{z}{\cos\theta}, \rho = z\tan\theta$ (cf. Fig. 14) the two asymptotical presentations are comparable. This comparison leads to the statement $k(z) \sim K z^{\lambda - \frac{1}{2}}$. From this relationship the crack propagation near the origin O can be characterized. If the real part of λ is smaller than 0.5, $k(z)$ becomes unbounded from z to 0. Therefore, $k(z)$ is significantly larger near O than that at the rest of the crack front. So local crack growth is expected even for a very small load, as it is illustrated in Fig. 15.
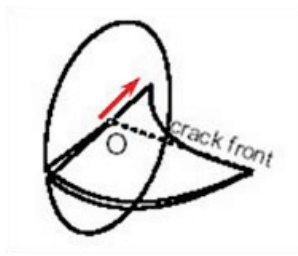
Figure 15: Explosion of the crack front.

For the real part of λ $\text{Re}(\lambda) > \frac{1}{2}$, $k(z)$ becomes 0 from z to 0. It means a weak corner singularity is present. That means the crack front is growing at the edge but not at the re-entrant corner. These ideas are comparable with the paper of Legullion

et al. Legullion and Sanchez-Palencia (1992) and will be verified by experiments in this paper.

5   Determination of relevant fracture mechanics parameters

For points P on a smooth part of the 3D crack front, the wedge singularity is present and the stresses are defined as:

$$\sigma_{ij}(r,\varphi,P) = \sum_{M=I}^{III} \frac{K_M(P)}{\sqrt{2\pi r}} f_{ij}^M(\varphi) + T_{ij} + O\left(\sqrt{r}\right) \tag{46}$$

with respect to a cylindrical coordinate system, cf. Fig. 16. In this equation, the fracture mechanics parameters - the so called stress intensity factors along the crack front - are K_I, K_{II} and K_{III} as the classical ones.
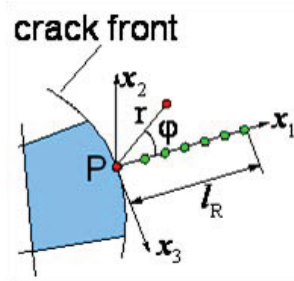
Figure 16: Wedge singularity.

Additionally, the T-stresses are considered in the Eq. (46), but at first only for the values different from 0. The fracture mechanical parameters are determined by using the regression function while minimizing the standard deviation for the angle $\varphi = 0$. Therewith the stress intensity factors along the edge are obtained with high accuracy Kuhn and Partheymuller (1999); Kolk and Kuhn (2001).

Next, the corner singularity is taken into account. The stresses for the corner singularity are expressed depending on a spherical coordinate system (cf. Fig. 17) via

$$\sigma_{ij}(\rho,\theta,\phi,O) = \sum_{L=1}^{3} K_L^* \rho^{\lambda_L - 1} f_{ij}^L(\theta,\phi) \tag{47}$$

Now, K_L^* denote the generalized stress intensity factors. By the utilization of the above performed asymptotic analysis, the common stress intensity factor can be
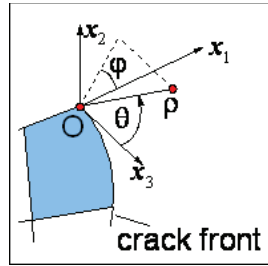
Figure 17: Corner singularity.

defined depending on the dominant eigenvalue λ_L. This leads to the statement($M = I, II, III$):

$$\lambda_L > 0.5 \quad \Rightarrow \quad K_M \to 0$$
$$\lambda_L = 0.5 \quad \Rightarrow \quad K_M$$
$$\lambda_L < 0.5 \quad \Rightarrow \quad K_M \to \infty$$

The determination of λ can be taken from some papers Bažant and Cedolin (1979); Dimitrov et al (2001); Dimitrov (2004); Dimitrov et al (2002a,b); Kolk et al (2003).

Based on above definition, it can be defined whether an explosion of the crack in the origin or the cease of crack or the situation such as a normal wedge singularity is present. In the next step, an incremental iterative procedure to find the crack propagation by simulation along the crack front including the asymptotic solution of the corner singular point O is described. Therefore, at first, a structure analysis based on BEM or FEM is done. The determination of the new crack geometry is based on a reliable 3D crack growth criterion. Then the numerical model has to be updated. It is started for local Mode-I conditions and it is looked for the constant energy released rate along the whole crack front for the problem with $\lambda_L = 0.5$. As a result, the wedge singularity along the whole crack front including the re-entrant corner point is obtained. This will be checked for a special problem - the surface intersection point of a 3D crack front (see Fig. 18).

From our structure analysis together with the requirements as a side condition of the constant energy released rate, the angle γ (cf. Fig. 19) is obtained in a very nice accuracy in comparison with the results from the past Pook (1992); Bažant and Cedolin (1979).

Additionally, some fatigue crack growth experiments in this direction have been done for the material PMMA with Young's modulus $E \approx 3.6\,\text{GPa}$ and Poisson's ratio $v \approx 0.365$.

From Fig. 20, the same value: $\gamma = 14°$ is obtained from experiments as well as from computational simulation.

Next, experiments of the same type have been done with a trapezoidal cross section Heyder et al (2005). For that problem, again a crack front intersection angle of $14°$ is obtained (cf. Fig. 21).

Prediction of the kink angle

For the prediction of the kink angle the maximum tangential stress criterion (MTS) can be used. Therefore, the following equations:

$$\text{Condition} \quad \frac{\partial \sigma_\varphi}{\partial \varphi} = 0 \tag{48}$$

$$\text{Restriction} \quad \frac{\partial^2 \sigma_\varphi}{\partial \varphi^2} < 0 \tag{49}$$

have to be fulfilled. The definition of σ_φ is illustrated in Fig. 22.

Following the last two equations (48) and (49), the kink angle using the MTS criteria is calculated directly via:

$$\varphi^{MTS} = 2\arctan\left\{ \frac{-2K_{II}}{K_I + \sqrt{K_I^2 + 8K_{II}^2}} \right\} \tag{50}$$

In complicated cases, K_{III} has to be considered additionally Schöllmann et al (2001); Richard et al (2001).

In this case the three equations:

$$\sigma_1^{cyl} = \frac{\sigma_\varphi + \sigma_{\tilde{x}_3}}{2} + \frac{1}{2}\sqrt{\left(\sigma_\varphi - \sigma_{\tilde{x}_3}\right)^2 + 4\tau_{\phi\tilde{x}_3}^2} \tag{51}$$

$$\frac{\partial \sigma_1^{cyl}}{\partial \varphi} = 0 \tag{52}$$

$$\frac{\partial^2 \sigma_1^{\text{cyl}}}{\partial \varphi^2} < 0 \tag{53}$$

have to be fulfilled. Now, the kink angle

$$\varphi^{3D} = f(K_I, K_{II}, K_{III}, \nu) \tag{54}$$

depends on the Poisson's ratio ν additionally because a 3D elasticity problem is present. For the illustration of this kink angle φ^{3D} and φ^{MTS} barycentric coordinates with the following definitions are utilized:

$$K_I^n = \frac{K_I}{K_I + |K_{II}| + |K_{III}|} \tag{55a}$$

$$K_{II}^n = \frac{|K_{II}|}{K_I + |K_{II}| + |K_{III}|} \tag{55b}$$

$$K_{III}^n = \frac{|K_{III}|}{K_I + |K_{II}| + |K_{III}|} \tag{55c}$$

Now, the T-stresses especially the element T_{11} is used in the MTS-criterion. Therefore, the following equation:

$$\sigma_{\varphi\varphi}(r, \varphi, P) = \sum_{M=\text{I}}^{\text{II}} \frac{K_M(P)}{\sqrt{2\pi r}} f_{\varphi\varphi}^M(\varphi) + T_{11}(\sin \varphi)^2 \tag{56}$$

is obtained for the stresses and the kink angle results in:

$$\varphi_0^{MTS} : \frac{\partial \sigma_{\varphi\varphi}}{\partial \varphi} = 0; \frac{\partial^2 \sigma_{\varphi\varphi}}{\partial \varphi^2} < 0 \qquad \Rightarrow \varphi^{MTS} = f(K_I, K_{II}, T_{11}, r) \tag{57}$$

Fig. 25 shows the deflection angle in barycentric coordinates by considering additionally the term from the T-stresses T_{11}.

The correction of the kink angle can be done by extending of the 3D-criterion with incorporation of all T-stresses. This goes back to Kolk et al (2003). The idea is to use the maximum principal stress on an imaginary cylindrical sphere around the crack front. The full 3D case the kink angle is obtained as follows:

$$\varphi_0^{3D} : \frac{\partial \sigma_1^{\text{cyl}}}{\partial \varphi} = 0; \frac{\partial \sigma_1^{\text{cyl}}}{\partial \varphi^2} < 0$$
$$\Rightarrow \varphi_0^{3D} = f(K_I, K_{II}, K_{III}, T_{11}, T_{13}, T_{33}, r, \nu) \tag{58}$$

The influence of all the parameters for getting the kink angle for the full 3D case is shown in Fig. 26.

6   Numerical and experimental results

At first, a two dimensional problem as an interface crack is studied. Here, the situation of two different materials perfectly connected is present, see Fig. 27. The interfacial crack is located between carbon fibers and carbon matrix in simulation. The material data are given by:

$$E_I = 200\,\text{GPa}$$
$$E_{II} = 22\,\text{GPa}$$
$$\frac{E_L}{E_{II}} \approx 10$$

It means the Young's modulus shows a quotient of E_I and E_{II} is approximate 10. The Poisson's ratio for that problem is $\nu \approx 0.2$.

The dominant eigenvalue λ for different angles α is computed with the presented method. As shown in Fig. 27, the corner point singularities for the angles 20°, 55° and 190° have to be evaluated. The results for this problem can be taken from Fig. 28. Within this figure the dominant eigenvalues of the angles under consideration are marked with a star.

By the utilization of the dominant eigenvalues, it can be decided whether a critical crack grows or the crack front stops under static as well as fatigue conditions. This solution can be compared with Glushkov et al (1999).

In the next problem, a 3 point bending specimen is investigated as schematically shown in Fig. 29. Here, the surface breaking point of the crack front on a traction free surface is analyzed.

At first, the strain energy released rate values G_I, G_{II} and G_{III} are determined by the 3D finite element analysis (see Fig. 29). These graphs are very carefully computed from the results by the group of F. G. Buchholz [1]. It is not quite clear from this 3D finite element analysis what happens on the free surface. All the three curves stop with finite values.

As a result of the analysis for the dominant eigenvalues the values are obtained.

$$\lambda_1 = 0.393$$
$$\lambda_2 = 0.679$$
$$\lambda_3 = 0.978$$

Therewith, the criteria for crack growth can be evaluated. According to this criterion, G_{II} and G_{III} must go to ∞ when values for z/t with the limit to 0.5 (crack front

---

[1] see Acknowledgements

surface breaking point). The eigenvalue shows us that these values of the crack tip are strong and the values must go to unbounded values for G_{II} and G_{III}.

For the weak singular mode, the eigenvalue $\lambda_2 = 0.679$ is obtained and for mode I of the free surface G_I tends to zero:

$$G_I \to 0 \quad \text{for} \quad z/t \to 0.5.$$

Overall, it can be found that the classical finite element method is not good enough to predict crack growing from aforementioned studies.

In the following, a 3D corner singularity in comparison with experimental data is studied. In detail, a crack in a four point bending specimen of the brittle and homogeneous material PMMA under fatigue loading conditions is considered (see Fig. 30).

Fatigue conditions are chosen because the behavior of the crack can be observed and analyzed step by step. In principle, the observed behavior-crack arrest, stable or unstable fatigue crack growth-can be transferred to static loading conditions if dynamic effects of fast static crack growth are negligible.

An overview about the experimental equipment for the four point bending test is given in Fig. 31. For the measurement of the crack propagation, a digital automatic identification as illustrated in Fig. 32 is utilized.

After the crack front has reached the trapezoid area, the specimen is modified in order to generate points with singularities different from 0.5. On the one hand a slit through the specimen is introduced; on the other hand the specimen has been cut in order to generate an unsymmetrical situation (cf. Fig. 33).

At first, the problem of the specimen with a slit is investigated. The experimental results are illustrated in the Figs. 34 - 36. Fig. 34 shows exemplarily photos of the initial crack front without the slit and of three crack shapes during crack propagation. In fig. 35 observed crack front shapes of the experiment with the number of load cycles are sketched. For two crack fronts analyses of distribution of the SIF along the crack are made. The results are plotted in Fig. 36. Here, hypothetical crack fronts of a constant distribution of the SIF compared to the experimental obtained ones are illustrated additionally. Although fatigue crack propagation is also a very interesting challenge special focus is on the behavior of the crack after inserting the slit within the present work. For details on the utilized numerical methods for determination of distribution of SIF as well as crack growth within this work seeHeyder and Kuhn (2006); Kolk and Kuhn (2005).
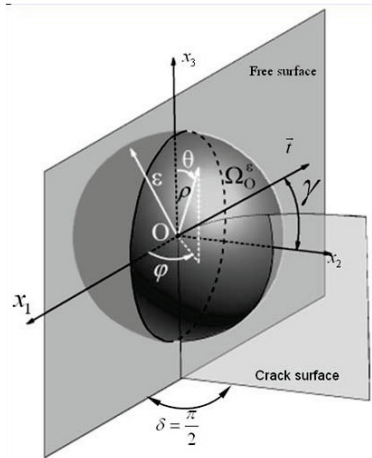
Figure 18: Geometry for determination of the crack front angle γ.
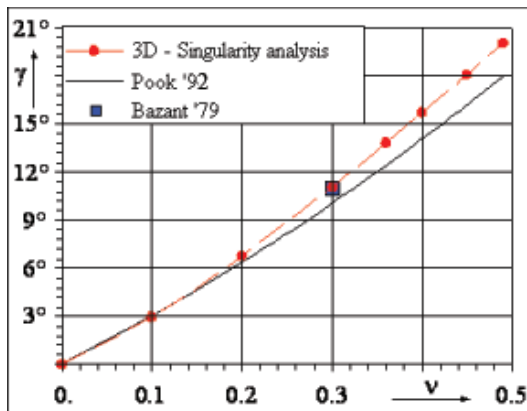
Figure 19: Crack front angle γ at the crack tip depending from υ(Poisson's ratio).
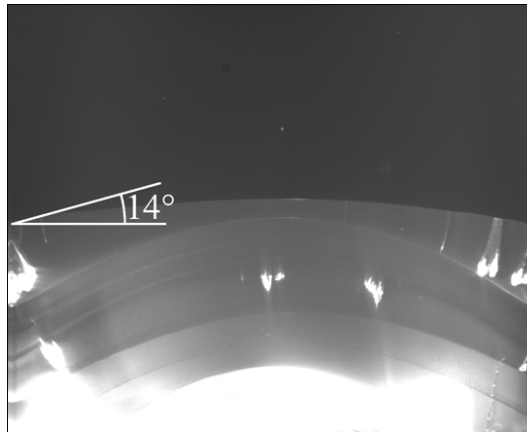
Figure 20: SEC specimen for determination of the crack tip angle γ.
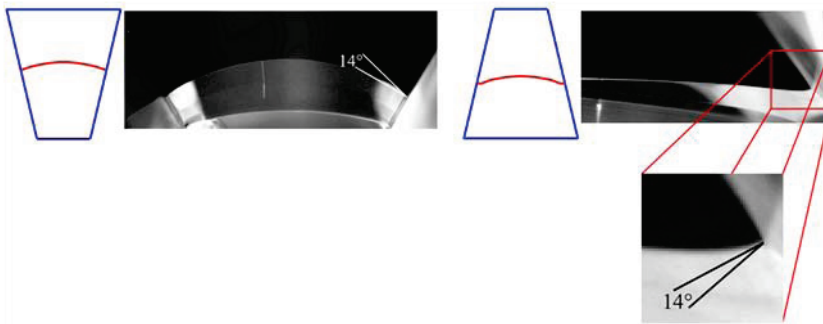
Figure 21: A trapezoidal cross section for determination of the crack front angle γ at the crack tip.
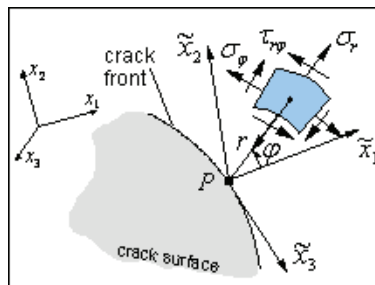
Figure 22: Definition of the coordinate system and the stresses for determination of the kink angle.
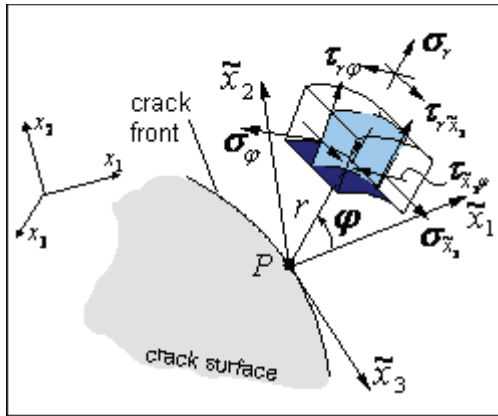
Figure 23: Stress definitions for prediction of the kink angle by considering K_{III}
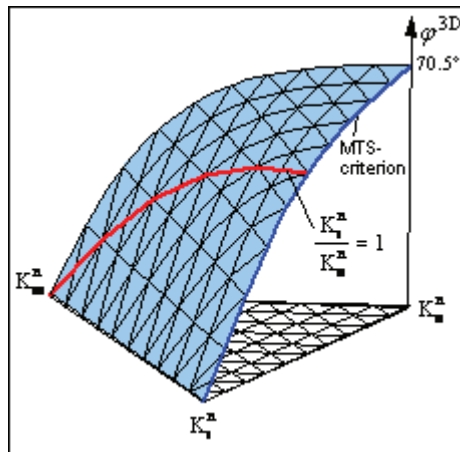
Figure 24: Graph for the kink angle φ 3D using the MTS criteria and the barycentric coordinates
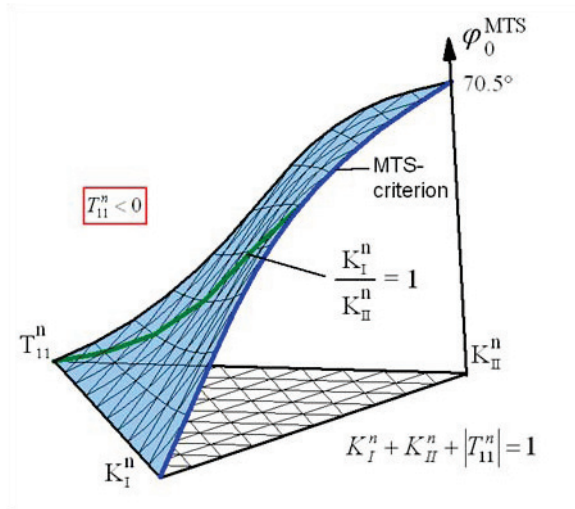
Figure 25: Illustration for definition of the kink angle ϕ_0^{MTS}
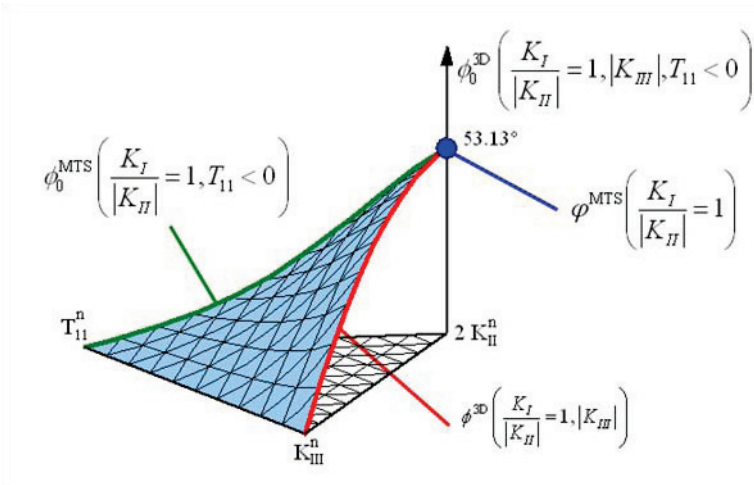
Figure 26: Influence of all the parameters for getting the kink angle for the full 3D case.
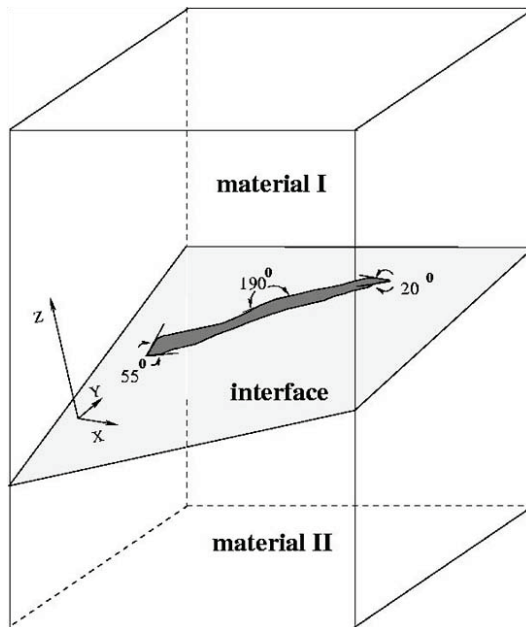
Figure 27: An interfacial crack between two materials.
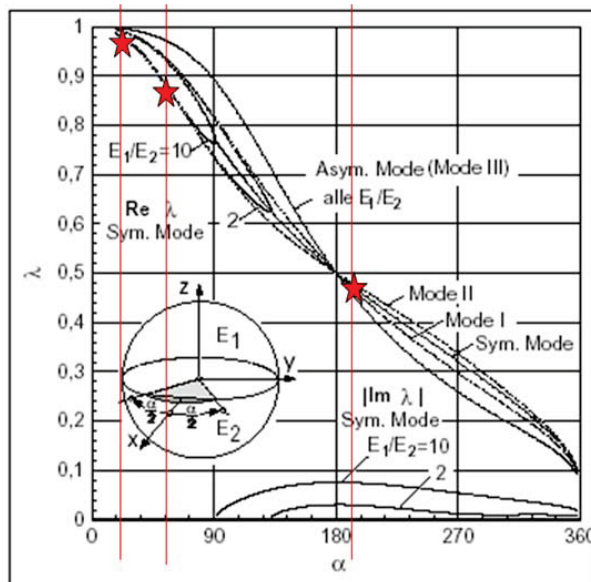
Figure 28: Three different angles and the dominant eigenvalues (marked with star).

a.   b.
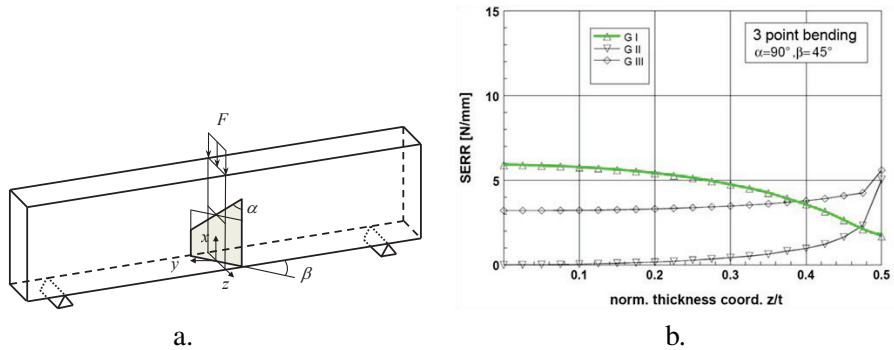
Figure 29: 3 point bending specimen(a) and its strain energy released rate (SERR)(b)
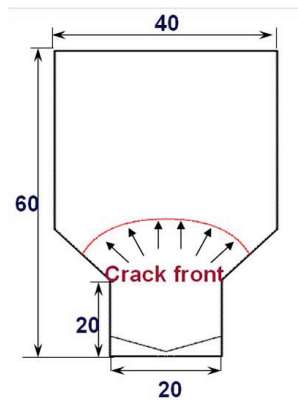
Figure 30: Definition of the specimen.

Figure 31: Four point bending test.
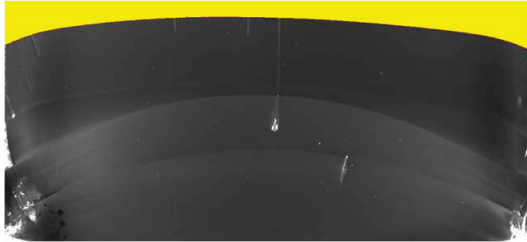
Figure 32: Evolution of crack propagation.
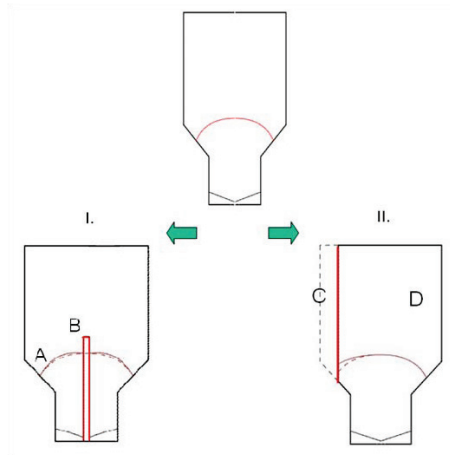
Figure 33: Three types of specimen are used for the experimental work and the additional numerical simulation.
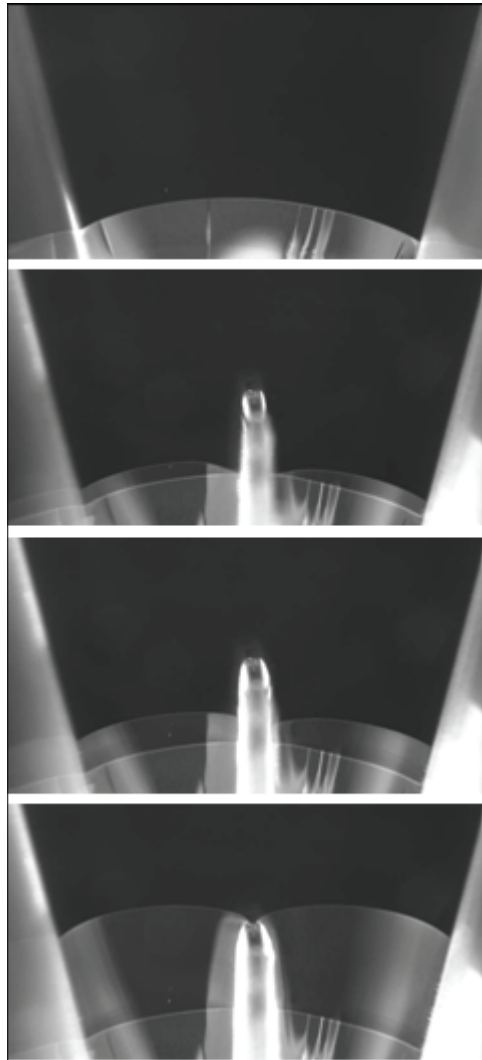
Figure 34: Crack growing for a specimen with a slit.
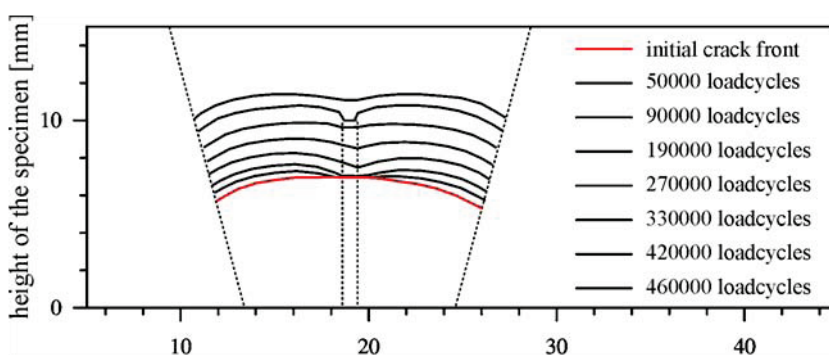
Figure 35: Specimen with crack front after cycling loadings with a unification of the two crack fronts.

After the manufacturing of the slit, the crack stops growing at the new generated surface breaking points in the experiment. The analysis of the dominant eigenvalues of this geometric situation shows that a weak singularity is present, which confirms the experimental observation. Since the crack grows inside the specimen the geometric situation at this point changes. Once the typical crack front intersection angle is reached at this point the crack starts growing even at this point.

Next, the unsymmetrical specimen is investigated. The crack growth up to 700,000 cycles on the servohydraulic testing machine is shown in Fig. 37.

On side C of this specimen the situation for a critical crack tip is present. With the analysis of the eigenvalues, it can be found that the crack grows very fast at the origin O as shown in the Fig. 37. until the geometric situation of the special crack front intersection angle with the classical stress singularity is present.

Fig. 38 shows the crack propagation of a corner crack in a four point bending specimen. Here, it can be found that the crack front grows very classically, cycle for cycle. But if the crack front comes in the near of the free surface, it can be shown that the dominant eigenvalue is a critical one and the crack tip grows under the influence of the corner singularity. The comparision between this experiment results and the simulation is shown in Fig. 38 which implies htat most results are very coincident.

Finally, a totally unsymmetrical crack in a four point bending specimen is analyzed. The reason for crack growth results in this case from another phenomenon. Here, only the stress intensity factor at the tip is dominant.

As shown in Fig. 39, the phase 1 of crack growth is a symmetrical one for crack initiation. In phase 2 and phase 3 unsymmetrical conditions are present during
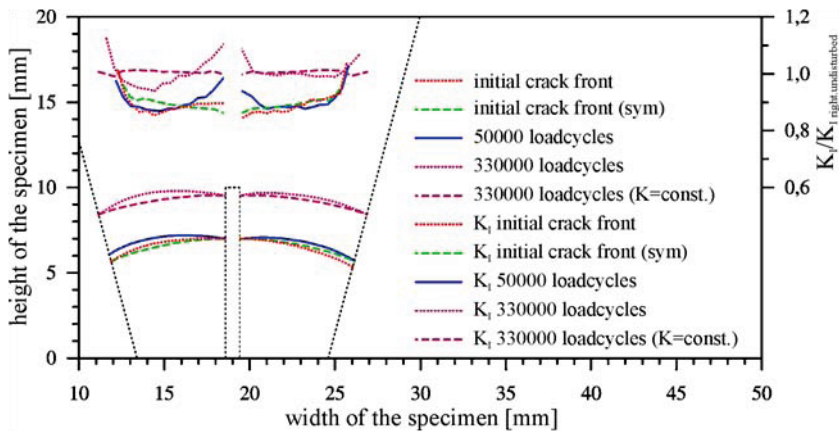
Figure 36: Crack growing with two different crack fronts along the slit of this specimen.
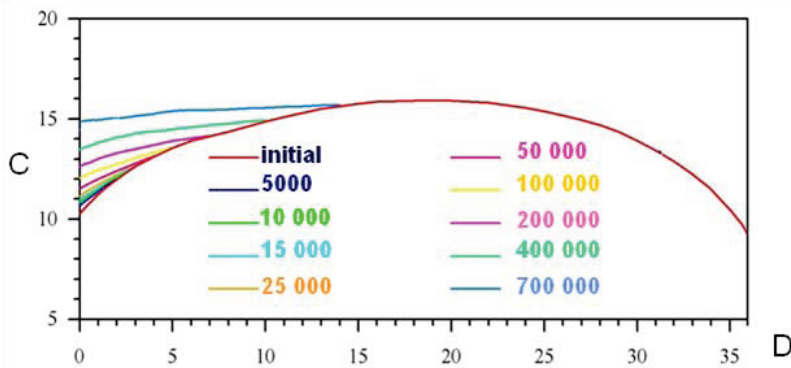
Figure 37: Crack growing for this unsymmetrical specimen.
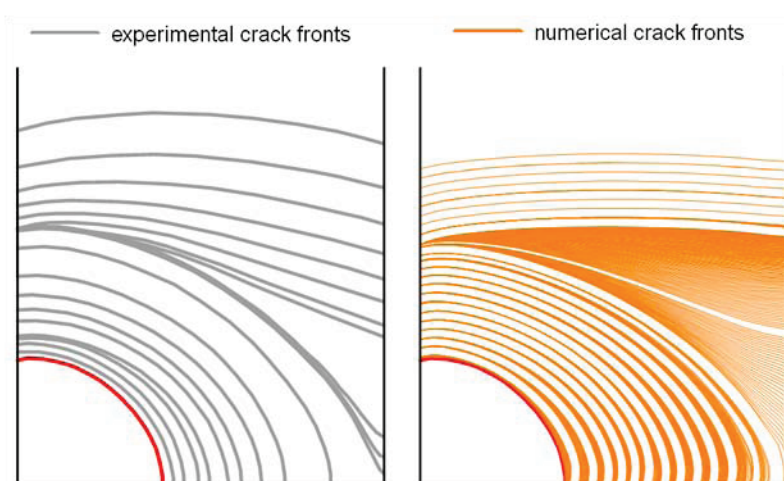
Figure 38: Experimental and numerical verification for a crack growing for an unsymmetrical specimen.
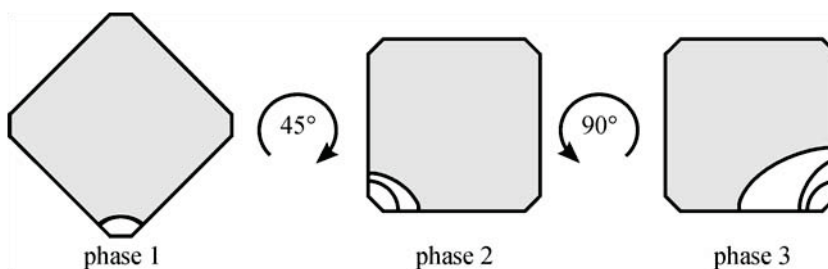
Figure 39: Four point bending specimen with phase 1 to phase 3.

crack growth. For this problem the reason for different crack propagation rates (cf. Figs. 40 and 41) is not that the dominant eigenvalue leads to a critical value. Here the reason is only the value of the stress intensity factor.

7 Conclusions

In this paper the importance of singularities in 3D fracture mechanics has been shown, and more especially the corner singularities have to be considered if the failure of concrete 3D structures was described. Fracture mechanics of very modern materials like composites is very difficult with many open questions until now. However, the first and the basis for answering these questions is to know the dom-
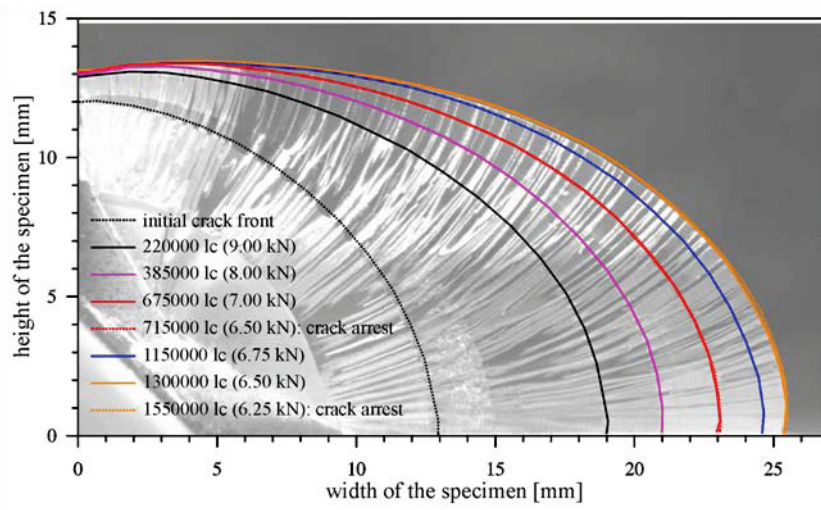
Figure 40: Experimental data for the crack front.
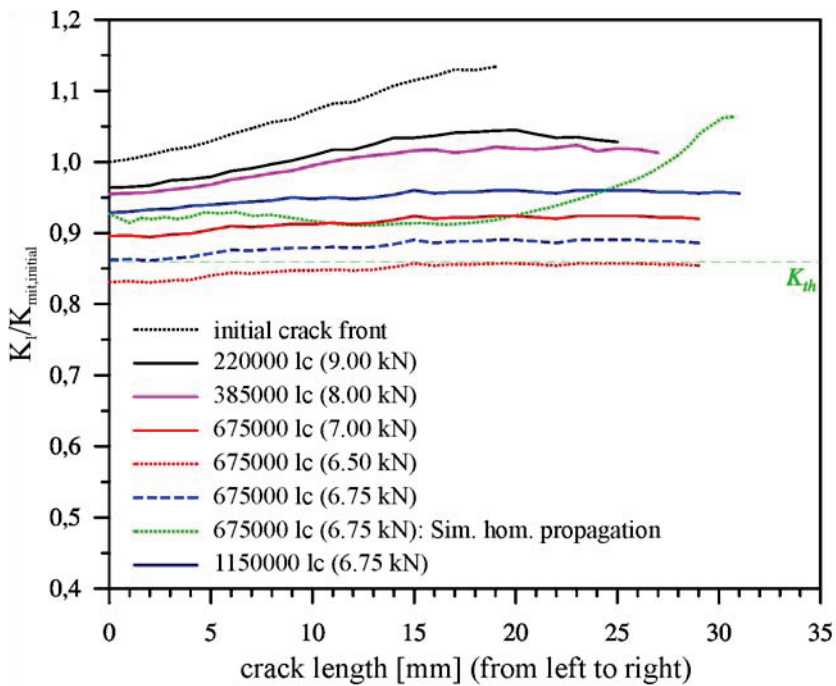
Figure 41: Crack length in mm from left to right with a normalized stress intensity factor.

inant eigenvalue at the crack tip in order to define criteria for the behavior of the crack.

Based on the Lemma of Kondratiev a Petrov-Galerkin finite element method has been presented to compute the dominant eigenvalue for that problem. The resulting quadratic eigenvalue problem has been solved by the Arnoldi method.

Additionally, the crack growing including the corner singularity for some important questions has been studied by computation. In comparison with experimental results it has been shown that corner singularities are important and are the reason for crack growing in a special manner.

References

Benthem, J. P. (1977): State of stress at the vertex of a quarter-infinite crack in half-space. *Int J Solids Struct*, vol. 13, pp. 479-492.

Smith, C. W.; Lloyd, W. R.; Rezvani, M.; Olaosebikan, O. (1986):   An Interpretation Boundary Effects in Cracked Bodies. *Proceeding of 13th South-eastern Conference on Theoretical and Applied Mechanics*, Columbia, South Carolina, pp. 359-366.

Smith, C. W.; Epstein, J. S.; Olaosebikan, O. (1986): Boundary Layer Effects in Cracked Bodies: An Engineering Assessment. ASTM special technical publication, vol. 17, pp. 775-778.

Smith, C. W.; Kobayashi, A. S. (1987): Experimental Fracture Mechanics. *In: Kobayashi A S(ed) Handbook on Experimental Mechanics*, Prentice-Hall Inc, Englewood Cliffs, NJ, pp. 891-956.

Smith, C. W.; Epstein, J. S.; Rezvani, M. (1989): Measurement of Dominant Eigenvalues in Cracked Body Problems. *Int J Fracture*, vol. 39, no. 1, pp. 1524-1535.

Schnack, E.; Becker, I.; Karaosmanoglu, N. (1990): Three-dimensional coupling of FEM and BEM in elasticity. In: Kuhn G, Mang H(eds) *Discretization Methods in Structural Mechanics*, Springer-Verlag, London, pp. 415-425.

Smith, C. W.; Kobayashi, A. S. (1986): Experimental fracture mechanics. In: Kobayashi A S (ed) *Handbook on Experimental Mechanics*, Prentice-Hall Inc, Englewood Cliffs, NJ, pp. 891-957.

Piat, R.; Reznik, B.; Schnack, E.; Gerthsen, D. (2004): Modeling of effective material properties of pyrolytic carbon with different texture degrees by homogenization method *Compos Sci Technol* vol. 64, no. 13-14, pp. 2015-2020.

Kondratiev, V. A. (1967): Boundary value problems for elliptic equations in domains with conical or angular points. *Trans Moscow Math Soc*, vol. 16, pp.227-313.

Legullion, D.; Sanchez-Palencia, E. (1992): Fracture in heterogeneous materials. In: Ladeveze P, Zienkiewicz O C (eds) *New advances in Computational Structural Mechanics*, Elsevier, Amsterdam, New York, pp. 423-434.

Kuhn, G.; Partheymuller, P. (1999): 3D crack growth simulations wiht the boundary element method. In: Sarler B, Brebbia C A, Power H (eds) *Moving Boundaries V-Computational Modelling of Free and Moving Boundary Problems*, WIT Press, Southampton, pp. 69-78.

Kolk, K.; Kuhn, G. (2001): 3D crack growth simulation. In: Waszczyszyn Z, Pamin J (eds) *Proceedings of the 2nd European Conference on Computational Mechanics*, Cracow, Poland.

Bažant, Z. P.; Cedolin, L. (1979): Blunt crack band propagation in finite element analysis. *J. Engng Mech. Div. ASCE*, vol. 105, pp. 297-315.

Dimitrov, A.; Andra, H.; Schnack, E. (2001): Efficient computation of order and mode of corner singularities in 3D -elasticity. *Int J Num Meth Eng*, vol. 52, pp. 805-827.

Dimitrov, A. (2004): On singularities in the solution of three-dimensional stokes flow and incompressible elasticity problems with corners. *Int J Num Meth Eng*, vol. 60, pp. 773-801.

Dimitrov, A.; Andra, H.; Schnack, E. (2002): Singularities near three-dimensional corners in composite laminates. *Int J Fracture*, vol. 115, pp. 361-375.

Dimitrov, A.; Buchholz, F. G.; Andra, H.; Schnack, E. (2002): Free-surface efects in crack propagation: a theoretical-numerical-experimental correlation. *Institute of Solid Mechanics, Karlsruhe Institute of Technology (KIT)*.

Kolk, K.; Mishuris, G.; Kuhn, G. (2003): Singularities with application to fatigue crack growth propagation. In: Movchan A (ed) *IUTAM Symposium on Asymptotics,Singularities and Homogenisation in Problems of Mechanics*. Kluwer, Dordrecht, pp. 433-443.

Pook, L. P. (1992): A brief introduction to fracture mechanics and the role of NDT. *Br J Non-destruct Testing*, vol. 34, pp. 595-600.

Bažant, Z. P.; Cedolin, L. (1979): Blunt crack band propagation in finite element analysis. *J Eng Mech Div ASCE*, vol. 105, pp. 297-315.

Heyder, M., Kolk, K.; Kuhn, G. (2005): Numerical and experimental investigations of the influence of corner singularities on 3d fatigue crack propagation. *Eng Fract Mech*, vol. 72, no. 13, pp. 2095-2105.

Schöllmann, M.; Kullmer, G.; Fulland, M.; Richard, H. A. (2001): A new criterion for 3D crack growth under mixed-mode (I+II+III) loading. In: Freitas M M (ed) *Proceedings of the 6th International Conference on Biaxial/Multiaxial Fatigue and Fracture*. Lisboa, Portugal, June 2001 vol. II, Instituto Superior Tecnico, pp. 598-596.

Richard, H. A.; Schöllmann, M.; Fulland, M.; Sander, M. (2001): Experimental and numerical simulation of mixed-mode crack growth. In: Freitas M M (ed) *Proceedings of the 6th International Conference on Biaxial/Multiaxial Fatigue and Fracture*. Lisboa, Portugal, June 2001 vol. II, Instituto Superior Tecnico, pp. 623-630.

Glushkov, E.; Glushkova, N.; Lapina, O. (1999): 3-D elastic stress singularity at polyhedral corner points. *Int J Solids Struct*, vol. 36, no. 8, pp. 1105-1128.

Apel, T. (2001): private communication.

Heyder, M.; Kuhn, G. (2006): 3D fatigue crack propagation: Experimental studies. *Int J Fatigue*, vol. 28, no. 5-6, pp. 627-634.

Kolk, K.; Kuhn, G. (2005): A predictor-corrector scheme for the optimization of 3D crack front shapes. *Fatigue Fract Eng Mater Struct*, vol. 28, pp. 117-126.